IRS-Assisted Wireless Powered NOMA: A Multi-band Scenario

Gabriela Albuquerque dos Santos, Francisco Xavier de Araújo Sobrinho, Francisco Rafael Marques Lima

***Abstract*— Wireless Powered Communication Networks (WPCNs) enable low-cost devices to harvest energy and transmit data wirelessly, yet face coverage and efficiency limitations. Intelligent Reflecting Surfaces (IRSs) emerge as a promising solution to enhance both Downlink Wireless Power Transfer (DL WPT) and Uplink Wireless Information Transmission (UL WIT) by intelligently reconfiguring the propagation environment. This paper studies the deployment of a single IRS to enhance the performance of WPCNs operating at different frequencies. We propose a joint optimization framework for IRS phase-shift configuration and resource allocation using Non-Orthogonal Multiple Access (NOMA) with Successive Interference Cancellation (SIC). Our solution assigns a determined number of ideal phase-shifts per WPCN while fixing the remaining on 0/2π. Results show significant sum-rate gains and highlight performance gaps for future improvements.**

***Keywords*— IRS, Wireless Powered Networks, Multi-band, NOMA.**

I. Introduction

Intelligent Reflecting Surface (IRS) technology is a promising component of future wireless communication systems. By intelligently reflecting signals, it dynamically reconfigures the wireless propagation environment, going beyond traditional transceiver optimization [1].

IRSs can improve not only conventional wireless networks but also Internet of Things (IoT) systems with strict energy constraints. In a Wireless Powered Communication Network (WPCN), low-cost devices like battery-free sensors harvest energy via Wireless Power Transfer (WPT) in the first stage and transmit data in the second one. IRSs enhance both energy harvesting and data transmission efficiency in this context [2].

Non-Orthogonal Multiple Access (NOMA) is also a promising technology that offers enhanced multiplexing gains in wireless networks when compared to Orthogonal Multiple Access (OMA). It transmits multiple signals simultaneously using superposition coding. Receivers apply Successive Interference Cancellation (SIC) to decode signals in a specific order. Incorporating NOMA into the data transmission stage of a WPCN enhances spectral efficiency and system fairness [3].

In recent years, numerous studies have investigated the use of IRSs for energy harvesting. In [4], the authors address total data rate maximization in a WPCN-NOMA system aided by an IRS. Their optimization adjusts transmit power, stage durations, and IRS phase-shifts for both stages. Results show that IRSs significantly enhance the performance of WPCN systems.

While [4] considers distinct phase-shifts for the IRS in each stage, [5] shows that the same phase-shifts can be used in both stages, with no loss of optimality, reducing signaling overhead. An Alternating Optimization (AO) approach is applied to jointly optimize time allocation and phase-shifts for rate maximization in an IRS-assisted WPCN-NOMA system.

In [6] the authors apply the method developed in [5] to maximize data rates and meet Quality of Service (QoS) requirements while using Genetic Algorithm (GA) as opposed to AO. Using the same assumption, [7] investigates the deployment of several IRSs in order to maximize the data rates of one single WPCN.

Beyond energy harvesting applications, [8] proposes a practical IRS model for multi-band, multi-cell networks. This simplified model supports realistic IRS integration. Simulations reveal significant gains in power efficiency and rate via joint beamforming and reflection optimization. Building on this model, [9] incorporates Rate-Splitting Multiple Access (RSMA) to maximize sum-rates.

Although most of current works focus on single-band IRS designs, we propose a spectrally efficient alternative where one multi-band IRS simultaneously supports several co-located WPCNs. This enables a single surface to serve heterogeneous networks via intelligent phase-shift adaptation across bands, avoiding multiple dedicated installations. Our IRS-aided NOMA-WPCN system addresses this multi-band scenario through (1) joint optimization of WPT/WIT time intervals and multi-band phase-shifts, and (2) introduction of a selection matrix that optimally allocates reflecting elements to specific bands for total data rate maximization.

The remainder of this article is structured as follows. Section II introduces the system model along with the key assumptions. The problem under investigation is formulated in Section III, and corresponding solution approaches are detailed in Section IV. Section V presents a performance evaluation of the proposed algorithms and provides a discussion of the results. Finally, the main conclusions are summarized in Section VI.

Notation: Assume that $(\cdot)^T$ and $(\cdot)^H$ represent the transposed operator and the transposed conjugate (Hermitian) operator, respectively. The symbol $\odot$ represents the element-wise product operator. a_n represents the n-th element of vector $\mathbf{a}$. $\|\mathbf{a}\|_0$ denotes the number of nonzero elements in vector $\mathbf{a}$. $\mathbb{C}^{M\times N}$ represents the subspace of $M \times N$ dimensional complex matrices. The operation $\text{diag}\,(\mathbf{v})$ returns a diagonal matrix with vector $\mathbf{v}$ in the main diagonal.

Gabriela A. dos Santos and Francisco X. A. Sobrinho are affiliated with the Federal University of Ceará, Sobral campus, Sobral-CE, Brazil. Francisco R. M. Lima is affiliated with the Postgraduate Program in Electrical and Computer Engineering (PPGEEC), Sobral campus, Federal University of Ceará, Sobral-CE, Brazil, and with the Wireless Telecommunications Research Group (GTEL), Fortaleza-CE, Brazil. E-mails:{gabriela.albuquerque, xavier.araujo99}@alu.ufc.br and rafaelm@gtel.ufc.br.

II. System Model

The proposed system consists of an IRS-assisted multi-band WPCN. The IRS, which is composed of N reflecting elements, is deployed to assist the Uplink Wireless Information Transmission (UL WIT) and the Downlink Wireless Power Transfer (DL WPT) in S WPCNs or cells[1], simultaneously. The s-th cell is served by a single-antenna Hybrid Access Point (HAP) that serves K_s wireless-powered devices, also with a single antenna each, at a frequency f_s. Let $\mathcal{S} \triangleq \{1, \ldots, S\}$ represent the set of HAPs, $\mathcal{K}_s \triangleq \{1, \ldots, K_s\}$, the set of devices served by the s-th HAP, and $\mathcal{N} \triangleq \{1, \ldots, N\}$, the set of IRS reflecting elements. With no loss of generality, we assume $f_1 > f_2 > \cdots > f_S$ in this multi-band scenario.

In WPCN system, each time frame is divided into two distinct stages: stage 1, when occurs the DL WPT, and stage 2, when the UL WIT happens. Let $t_{0,s}$ and $t_{1,s}$ represent the durations of stages 1 and 2 for the s-th HAP, respectively, such that $t_{0,s} + t_{1,s} = T$, where T denotes the total time frame length, which is assumed to be the same for all WPCNs. We assume that T is sufficiently short so that the channel coefficients of all relevant links remain constant during the entire frame. Additionally, channel reciprocity between uplink and downlink is assumed for all communication links. This enables the use of uplink training to acquire downlink Channel State Information (CSI) at the transmitter. The channel coefficients are defined as follows: $\mathbf{g}_s \in \mathbb{C}^{N\times 1}$ represents the channel vector from the s-th HAP to the IRS; $\mathbf{h}_{\mathrm{r},s,k_s}^H \in \mathbb{C}^{1\times N}$ denotes the channel vector from the IRS to the k_s-th device; and $h_{\mathrm{d},s,k_s} \in \mathbb{C}$ refers to the direct channel from the s-th HAP to its k_s-th device, where $s \in \mathcal{S}$ and $k_s \in \mathcal{K}_s$.

During DL WPT, each HAP transmits an energy signal at a constant power level P_{HAP} over a duration $t_{0,s}$. The contribution of noise energy is neglected for energy harvesting purposes, as it is significantly weaker than the signal received from the HAP. Furthermore, the impact of the practical reflection amplitude response can be considered negligible on the optimization of the proposed multi-band system [10]. In this manner, we will assume that all phase-shift amplitudes have unit modulus. Let $\mathbf{\Theta}_s = \mathrm{diag}(e^{j\theta_{s,1}}, \ldots, e^{j\theta_{s,N}})$ denote the reflection phase-shift matrix of the IRS for DL WPT, where $\theta_{s,n} \in [0, 2\pi), \forall s \in \mathcal{S}$ and $\forall n \in \mathcal{N}$.

Accordingly, the harvested energy at device k_s is given by:

$$E_{k_s}^{\mathrm{h}} = \eta P_{\mathrm{HAP}} |h_{\mathrm{d},s,k_s} + \mathbf{h}_{\mathrm{r},s,k_s}^H \mathbf{\Theta}_s \mathbf{g}_s|^2 t_{0,s}, \tag{1}$$

$$E_{k_s}^{\mathrm{h}} = \eta P_{\mathrm{HAP}} |h_{\mathrm{d},s,k_s} + \mathbf{q}_{s,k_s}^H \mathbf{v}_{0,s}|^2 t_{0,s}, \tag{2}$$

where $\eta \in (0, 1]$ is the energy conversion efficiency, which was made equal for all devices. Furthermore, we define $\mathbf{q}_{s,k_s}^H = \mathbf{h}_{\mathrm{r},s,k_s}^H \mathrm{diag}(\mathbf{g}_s)$ and $\mathbf{v}_{0,s} = [e^{j\theta_{s,1}}, \ldots, e^{j\theta_{s,N}}]^T$.

NOMA is applied for stage 2, therefore, all k_s devices simultaneously transmit information signals to the s-th HAP during time $t_{1,s}$ with transmit power p_{k_s}, $\forall k_s \in \mathcal{K}_s$. Without loss of generality, assuming that the devices are sorted in ascending order according to their index, perfect SIC is performed at the HAPs. So, in order to decode the message from device $j \in \mathcal{K}_s$, the HAP $s \in \mathcal{S}$ needs to previously decode the message from device $i \in \mathcal{K}_s$ with $i < j$, and cancel it from the total received signal, following $i = 1, 2, \ldots, j-1$. The additive white Gaussian noise power is denoted by σ^2 and the phase-shift vector for stage 2 is, as proven in [5], the same used for stage 1, $\mathbf{v}_{0,s}$. In that way, the achievable throughput of device k_s, in bits/s/Hz, is given by

$$r_{k_s} = t_{1,s} \log_2 \left(1 + \frac{p_{k_s} |h_{\mathrm{d},s,k_s} + \mathbf{q}_{s,k_s}^H \mathbf{v}_{0,s}|^2}{\sum_{i=k_s+1}^{K_s} p_i |h_{\mathrm{d},s,i} + \mathbf{q}_{s,i}^H \mathbf{v}_{0,s}| + \sigma^2} \right). \tag{3}$$

Finally, the sum throughput for all devices is expressed as

$$R_{\mathrm{T}} = \sum_{s=1}^{S} \sum_{k_s=1}^{K_s} r_{k_s}$$

$$\overset{(a)}{=} \sum_{s=1}^{S} t_{1,s} \log_2 \left(1 + \sum_{k_s=1}^{K_s} \frac{p_{k_s} |h_{\mathrm{d},s,k_s} + \mathbf{q}_{s,k_s}^H \mathbf{v}_{0,s}|^2}{\sigma^2} \right), \tag{4}$$

where the equality (a) can be deduced from [11].

A. Practical IRS Reflection Model

Following the practical IRS reflection model proposed in [8], each IRS reflecting element is controlled by its variable capacitance, and the same reflecting element exhibits different phase-shift responses to signals at different frequency bands. In that matter, when considering three different frequencies sufficiently parted from each other, being $f_1 > f_2 > f_3$, there will be three different capacitance ranges C_1, C_2 and C_3, where each of these will provide an ideal $(0, 2\pi]$ phase-shift for one of the frequencies, while being able to serve a fixed $0/2\pi$ phase-shift for the others.

This frequency-selective behavior of each reflecting element makes it possible to model the practical phase-shift response as the product of an ideal phase-shift and a binary selection variable. Thus, for the n-th reflecting element, we denote its service selection vector as $\mathbf{a}_n \triangleq [a_{1,n}, \ldots, a_{S,n}]^T$, $a_{s,n} \in \{0, 1\}$. Furthermore, $a_{s,n} = 1$ represents that the s-th HAP is selected to be served with a fully tunable phase-shift response provided by the n-th reflecting element of the IRS, and $a_{s,n} = 0$ indicates that the n-th reflecting element exhibits a fixed $0/2\pi$ phase-shift for the s-th HAP. Moreover, according to the above analysis, each reflecting element can serve, at most, one single HAP. Therefore, the constraint for the service selection vector of the n-th reflecting element can be written as

$$\|\mathbf{a}_n\|_0 \leq 1, \quad a_{s,n} \in \{0, 1\}, \quad \forall s, n. \tag{5}$$

We further specify a $S \times N$ service selection matrix for the IRS as $\mathbf{A} \triangleq [\mathbf{a}_1, \ldots, \mathbf{a}_N]$. It is noted that the s-th row of $\mathbf{A}$ is also the service selection vector for the s-th HAP and indicates which reflecting elements serve this HAP. For conciseness, we denote the service selection vector for the s-th HAP as $\tilde{\mathbf{a}}_s \triangleq [a_{s,1}, \ldots, a_{s,N}]^T \in \{0, 1\}^N$, which implies that

$$\mathbf{A} = [\mathbf{a}_1, \ldots, \mathbf{a}_N] = [\tilde{\mathbf{a}}_1, \ldots, \tilde{\mathbf{a}}_S]^T. \tag{6}$$

[1]The term 'cell' here denotes an independent WPCN (HAP + devices) and should not be confused with the classical cellular concept of frequency reuse or hexagonal cell partitioning.

The ideal phase-shift vector for the s-th HAP[2] can be denoted as $\boldsymbol{\phi}_s = [\phi_{s,1}, \ldots, \phi_{s,N}]^T$, $\phi_{s,n} \in (0, 2\pi]$. The practical phase-shift $\angle \mathbf{v_{0,s}}$ is, therefore, given by

$$\angle \mathbf{v_{0,s}} = \boldsymbol{\phi}_s \odot \tilde{\mathbf{a}}_s. \tag{7}$$

Consequently, the practical reflection vector for the s-th HAP can be expressed as $\mathbf{v_{0,s}} = \exp(j \angle \mathbf{v_{0,s}})$, as all amplitudes have unit modulus. Based on this, the practical IRS reflection model is given by:

$$\mathbf{v_{0,s}} = \exp\left(j\boldsymbol{\phi}_s \odot \tilde{\mathbf{a}}_s\right), \quad \forall s, \tag{8a}$$
$$\phi_{s,n} \in (0, 2\pi], \quad \forall s, n, \tag{8b}$$
$$\|\mathbf{a}_n\|_0 \leq 1, \quad a_{s,n} \in \{0, 1\}, \quad \forall s, n. \tag{8c}$$

Given the above system model and practical IRS reflection model, the total data rate maximization problem based on the optimization of the time length for stages 1 and 2, the IRS phase-shifts and the selection matrix of reflecting elements for each HAP will be formulated in Section III.

III. Problem Formulation

Under the described system model, knowing that the energy transmitted in stage 2, $p_{k_s} t_{1,s}$, can't exceed the energy harvested in stage 1, (2), the sum-rate maximization problem is formulated as

(P1):

$$\max_{\substack{t_{0,s}, t_{1,s}, \\ \boldsymbol{\phi}_s, \forall s, \mathbf{A}}} \sum_{s=1}^{S} t_{1,s} \log_2\left(1 + \sum_{k_s=1}^{K_s} \frac{t_{0,s} P_{\text{HAP}} \eta |h_{\text{d},s,k_s} + \mathbf{q}_{s,k_s}^H \mathbf{v}_{0,s}|^4}{t_{1,s}\sigma^2}\right) \tag{9a}$$

$$s.t. \quad t_{0,s} + t_{1,s} = T, \tag{9b}$$
$$t_{0,s} > 0,\ t_{1,s} > 0, \quad \forall k_s \tag{9c}$$
$$|[\mathbf{v}_{0,s}]_n| = 1, \quad \forall s, n \tag{9d}$$
$$\mathbf{A} = [\mathbf{a}_1, \ldots, \mathbf{a}_N] = [\tilde{\mathbf{a}}_1, \ldots, \tilde{\mathbf{a}}_S]^T, \quad \forall s, n \tag{9e}$$
$$\mathbf{v}_{0,s} = \exp\left(j\boldsymbol{\phi}_s \odot \tilde{\mathbf{a}}_s\right), \quad \forall s \tag{9f}$$
$$\phi_{s,n} \in (0, 2\pi], \quad \forall s, n \tag{9g}$$
$$\|\mathbf{a}_n\|_0 \leq 1, \quad a_{n,s} \in \{0, 1\}, \quad \forall s, n \tag{9h}$$
$$\|\tilde{\mathbf{a}}_s\|_0 = \frac{N}{S},\ \tilde{a}_{s,n} \in \{0, 1\},\ \frac{N}{S} \in \mathbb{N}^*,\ \forall s, n. \tag{9i}$$

In (P1), (9b) represents the total time constraint, (9c) the non-negativity constraint for the time duration of stages 1 and 2, and (9d) the unit-modulus constraint for the practical phase-shifts employed in both stages. (9e) defines the selection matrix $\mathbf{A}$. (9f) expresses that the practical phase-shift vector is the element-wise product between the ideal phase-shift vector and the selection vector for the s-th HAP. (9g) constrains the phase range for the ideal phase-shift vector. (9h) and (9i) determine the maximum number of HAPs that can be served by a single reflecting element with optimal phase-shift, and the exact number of reflecting elements required to serve each HAP with optimal phase-shift, respectively.

[2]By ideal phase-shift vector of the s-th HAP we mean the best phase-shift configuration of the IRS to maximize the total data rate in the s-th WPCN assuming that all IRS elements are serving WPCN s.

IV. Proposed Solution

The proposed solution is composed of two stages: the first consists of finding all N ideal phase-shifts as well as the ideal time durations $t_{0,s}$ and $t_{1,s}$ for each of the HAPs; in the second, we find a version of $\mathbf{A}$ that maximizes the total sum data rate of all S HAPs. Let $\mathbf{z}_s = [e^{j\phi_{s,1}}, \ldots, e^{j\phi_{s,N}}]^T$.

A. Proposed AO for $\mathbf{z}_s$, $t_{0,s}$ and $t_{1,s}$

For each HAP, i.e, with a fixed s, the following problem can be rewritten from (P1):

(P2):

$$\max_{\substack{t_{0,s}, t_{1,s}, \\ \mathbf{z}_s}} t_{1,s} \log_2\left(1 + \sum_{k_s=1}^{K_s} \frac{t_{0,s} P_{\text{HAP}} \eta |h_{\text{d},s,k_s} + \mathbf{q}_{k_s}^H \mathbf{z}_s|^4}{t_{1,s}\sigma^2}\right) \tag{10a}$$

$$s.t. \quad t_{0,s} + t_{1,s} \leq T_{\text{T}} \tag{10b}$$
$$t_{0,s} \geq 0,\ t_{1,s} \geq 0 \tag{10c}$$
$$|[\mathbf{z}_s]_n| = 1,\ \forall n. \tag{10d}$$

Although (P2) remains non-convex, it can be tackled using an AO-based strategy. In this scheme, we initially fix $t_{0,s}$ and $t_{1,s}$ to solve for $\mathbf{z}_s$. Using the obtained $\mathbf{z}_s$, we then update $t_{0,s}$ and $t_{1,s}$. This alternating process is repeated until a convergence condition is satisfied.

Fixing $\mathbf{z}_s$, we reformulate the problem as:

(P2.1):

$$\max_{t_{0,s}, t_{1,s}} t_{1,s} \log_2\left(1 + \sum_{k_s=1}^{K_s} \frac{t_{0,s} P_{\text{HAP}} \eta |h_{\text{d},s,k_s} + \mathbf{q}_{s,k_s}^H \mathbf{z}_s|^4}{t_{1,s}\sigma^2}\right) \tag{11a}$$

$$s.t. \quad t_{0,s} + t_{1,s} \leq T_{\text{T}} \tag{11b}$$
$$t_{0,s} \geq 0,\ t_{1,s} \geq 0 \tag{11c}$$

Problem (P2.1) is convex [12] and, therefore, can be solved optimally using efficient solvers [13]. Conversely, when $t_{0,s}$ and $t_{1,s}$ are fixed, problem (P2) simplifies to:

$$\text{(P2.2):} \quad \max_{\mathbf{z}_s} \sum_{k_s=1}^{K_s} \alpha |h_{\text{d},s,k_s} + \mathbf{q}_{s,k_s}^H \mathbf{z}_s|^4$$
$$s.t. \quad |[\mathbf{z}_s]_n| = 1,\ \forall n, \tag{12a}$$

where $\alpha = \frac{t_{0,s} P_{\text{HAP}} \eta}{t_{1,s}\sigma^2}$.

Before solving (P2.2), the following definitions are considered. The term $|h_{\text{d},s,k_s} + \mathbf{q}_{s,k_s}^H \mathbf{z}_s|^2$ is rewritten as $|\bar{\mathbf{q}}_{s,k_s}^H \bar{\mathbf{z}}_s|^2$, where $\bar{\mathbf{q}}_{s,k_s}^H = [\mathbf{q}_{s,k_s}^H \ \ h_{\text{d},s,k_s}]$ and $\bar{\mathbf{z}}_s = [\mathbf{z}_s^H \ \ 1]^H$. Define $\mathbf{Q}_{s,k_s} = \bar{\mathbf{q}}_{s,k_s} \bar{\mathbf{q}}_{s,k_s}^H$. Then, (P2.2) becomes:

(P2.2')

$$\max_{\mathbf{z}_s} \sum_{k_s=1}^{K_s} \alpha |h_{\text{d},s,k_s} + \mathbf{q}_{s,k_s}^H \mathbf{z}_s|^4 = \sum_{k_s=1}^{K_s} \alpha (\bar{\mathbf{z}}_s^H \mathbf{Q}_{s,k_s} \bar{\mathbf{z}}_s)^2 \tag{13a}$$

$$s.t. \quad |[\mathbf{z}_s]_n| = 1,\ \forall n. \tag{13b}$$

Successive Convex Approximation (SCA) can be applied to solve problem (P2.2'). Accordingly, the k_s-th term of objective function (13a) is lower-bounded using a first-order Taylor approximation around a given point $\hat{\mathbf{z}}_s$ [5]:

$$(\bar{\mathbf{z}}_s^H \mathbf{Q}_{s,k_s} \bar{\mathbf{z}}_s)^2 \geq 2\hat{\mathbf{z}}_s^H \mathbf{Q}_{s,k_s} \hat{\mathbf{z}}_s (2\,\mathrm{Re}\{\hat{\mathbf{z}}_s^H \mathbf{Q}_{\mathbf{s},\mathbf{k_s}} \bar{\mathbf{z}}_s)\} - 2\hat{\mathbf{z}}_s^H \mathbf{Q}_{s,k_s} \hat{\mathbf{z}}_s + (\hat{\mathbf{z}}_s^H \mathbf{Q}_{s,k_s} \hat{\mathbf{z}}_s)^2 \quad (14)$$

Let's consider $C_{s,k_s} = (\hat{\mathbf{z}}_s^H \mathbf{Q}_{s,k_s} \hat{\mathbf{z}}_s)^2$. Substituting C_{s,k_s} in (14) we have that

$$\begin{aligned} &2C_k(2\,\mathrm{Re}\{\hat{\mathbf{z}}_s^H \mathbf{Q}_{\mathbf{s},\mathbf{k_s}} \bar{\mathbf{z}}_s\} - 2C_k) + (C_k)^2 \\ &= 4\,\mathrm{Re}\{C_{s,k_s} \hat{\mathbf{z}}_s^H \mathbf{Q}_{\mathbf{s},\mathbf{k_s}} \bar{\mathbf{z}}_s\} - 4C_{s,k_s}^2 + C_{s,k_s}^2 \\ &= 4\,\mathrm{Re}\{C_{s,k_s} \hat{\mathbf{z}}_s^H \mathbf{Q}_{\mathbf{s},\mathbf{k_s}} \bar{\mathbf{z}}_s\} - 3C_{s,k_s}^2. \end{aligned} \quad (15)$$

Substituting (15) in (13a), the updated objective function of (P.2.2') is given by

$$4\,\mathrm{Re}\left\{\left(\sum_{k=1}^{K} \alpha C_{s,k_s} \hat{\mathbf{z}}_s^H \mathbf{Q}_{\mathbf{s},\mathbf{k_s}}\right) \bar{\mathbf{z}}_s\right\} - 3\sum_{k=1}^{K} \alpha C_{s,k_s}^2. \quad (16)$$

As shown in [5], the optimal solution of (P2.2') with the objective in (16) is given by $\bar{\mathbf{z}}_s = e^{j\arg\beta}$, where $\beta = (\sum_{k=1}^{K} \alpha C_{s,k_s} \hat{\mathbf{z}}_s \mathbf{Q}_{s,k_s})^H$. According to the AO method, the phase-shifts and the duration of stage 1 are alternately updated until convergence, which is ensured since the objective of (P2) increases monotonically with respect to $t_{0,s}$ and $\mathbf{z}_s$, $\forall s \in \mathcal{S}$.

B. Optimization Problem for $\mathbf{A}$

After solving (P2) for $\mathbf{z}_s$, $t_{0,s}$ and $t_{1,s}$, $\forall s \in \mathcal{S}$, we can rewrite problem (P1) as:

(P3):

$$\max_{\mathbf{A}} \sum_{s=1}^{S} t_{1,s} \log_2\left(1+\sum_{k_s=1}^{K_s} \frac{t_{0,s} P_{\mathrm{HAP}} \eta |h_{\mathrm{d},s,k_s} + \mathbf{q}_{s,k_s}^H \mathbf{v}_{0,s}|^4}{t_{1,s}\sigma^2}\right) \quad (17a)$$

$$s.t. \quad |[\boldsymbol{v}_{0,s}]_n| = 1, \quad \forall s, n \quad (17b)$$

$$\mathbf{A} = [\mathbf{a}_1, \ldots, \mathbf{a}_N] = [\tilde{\mathbf{a}}_1, \ldots, \tilde{\mathbf{a}}_S]^T, \quad \forall s, n \quad (17c)$$

$$\boldsymbol{v}_{0,s} = \exp(j\boldsymbol{\phi}_s \odot \tilde{\boldsymbol{a}}_s), \quad \forall s \quad (17d)$$

$$\phi_{s,n} \in (0, 2\pi], \quad \forall s, n \quad (17e)$$

$$\|\boldsymbol{a}_n\|_0 \leq 1, \quad a_{n,s} \in \{0,1\}, \quad \forall s, n \quad (17f)$$

$$\|\tilde{\boldsymbol{a}}_s\|_0 = \frac{N}{S},\ \tilde{a}_{s,n} \in \{0,1\},\ \frac{N}{S} \in \mathbb{N}^*,\ \forall s, n. \quad (17g)$$

In (P3), the integer binary component present in $\mathbf{v}_{0,s}$ is being raised to the fourth power, which makes (P3) an integer non-linear programming problem and requires a very complex approach to solve it. In this manner, we relaxed (P3) so that it would be an integer linear problem:

(P4):

$$\max_{\mathbf{A}} \sum_{s=1}^{S} \mathbf{v}_{0,s} \sum_{k_s=1}^{K_s} \mathbf{q}_{s,k_s}^H \quad (18a)$$

$$s.t. \quad |[\boldsymbol{v}_{0,s}]_n| = 1, \quad \forall s, n \quad (18b)$$

$$\mathbf{A} = [\mathbf{a}_1, \ldots, \mathbf{a}_N] = [\tilde{\mathbf{a}}_1, \ldots, \tilde{\mathbf{a}}_S]^T, \quad \forall s, n \quad (18c)$$

$$\boldsymbol{v}_{0,s} = \exp(j\boldsymbol{\phi}_s \odot \tilde{\boldsymbol{a}}_s), \quad \forall s \quad (18d)$$

$$\phi_{s,n} \in (0, 2\pi], \quad \forall s, n \quad (18e)$$

$$\|\boldsymbol{a}_n\|_0 \leq 1, \quad a_{n,s} \in \{0,1\}, \quad \forall s, n \quad (18f)$$

$$\|\tilde{\boldsymbol{a}}_s\|_0 = \frac{N}{S},\ \tilde{a}_{s,n} \in \{0,1\},\ \frac{N}{S} \in \mathbb{N}^*,\ \forall s, n \quad (18g)$$

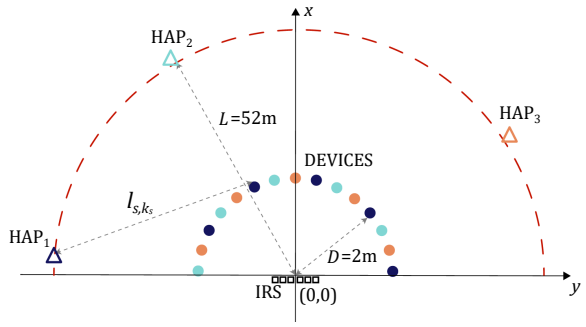

Fig. 1. An illustration of the relative position among the HAPs, IRS, and devices.

(P4) consists of a suboptimal approach, as it maximizes not the total data rate but the total gain from the reflected channels, which reflects on the data rate results. (P4) can be handled by an Integer Linear Program (ILP) solver, allowing the optimization process to conclude.

V. Simulation and Results

In this section, simulation results are presented to assess the impact of IRS deployment in multi-band scenarios, quantifying performance gains over conventional configurations and validating the proposed approach. We consider a multi-band system with $S = 3$ HAPs/WPCNs for the first simulation set and a variable S for the second. Each WPCN includes a single-antenna HAP serving $K_s = 5$ single-antenna devices, $\forall s$. In the first set, the IRS has a variable number of reflecting elements N, while in the second, it is fixed at $N = 180$. Noise power is $\sigma^2 = -85$ dBm and energy conversion efficiency is $\eta = 80\%$. Path loss exponents are set to 2.2 for HAP-IRS and IRS-device links, and 2.8 for HAP-device links [5].

Figure 1 shows the spatial layout. The IRS is at the origin $(0, 0)$, with HAPs randomly placed at a distance $L = 52$ m. Devices are randomly distributed $D = 2$ m from the IRS, as it primarily enhances edge device transmission.

Figs. 2 and 3 show the results of the first and second set of simulations, respectively, in which the convergence of the process described in section IV-A was safely achieved in 250 iterations. Our algorithm based on the proposed practical IRS reflection model in this paper is denoted as 'w/ IRS, proposed'. For performance benchmarking, we compare against three reference scenarios: First, the 'w/ IRS, w/o selection' case where all reflecting elements are dedicated to a single HAP with optimized phase-shifts while maintaining fixed 0° phase-shifts for other HAPs, representing a conventional single-band IRS deployment. Second, the 'w/ IRS, random selection' scheme where elements are randomly assigned to different HAPs with band-specific phase optimization, simulating uncoordinated resource allocation. Third, the IRS-less baseline ('w/o IRS') relying solely on direct links, which establishes the performance floor for our multi-band system.

Figure 2 demonstrates the spectral efficiency versus the number of IRS elements, N. All IRS-assisted schemes exhibit monotonically increasing sum-rates with growing N, while the "w/o IRS" baseline (showing the worst performance) remains flat, confirming the fundamental advantage of IRS deployment. Notably, our proposed scheme ("w/ IRS, proposed")

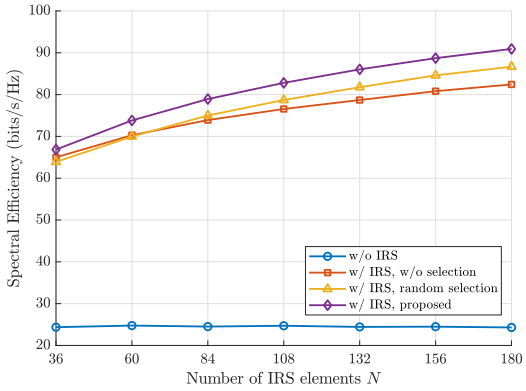

Fig. 2. Sum-rate versus the number of IRS reflecting elements N ($P_{\text{HAP}} = 40\text{dBm}, S = 3, K_s = 5$).

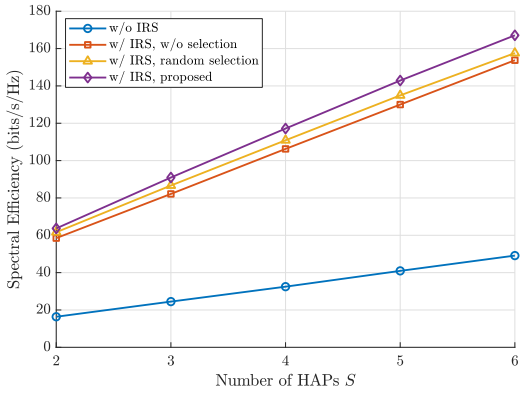

Fig. 3. Sum-rate versus the number of HAPs S ($P_{\text{HAP}} = 40\text{dBm}, N = 180, K_s = 5$).

consistently outperforms all benchmarks across all values of N, highlighting its scalability. The "w/ IRS, random selection" approach marginally surpasses the single-HAP dedicated scheme ("w/ IRS, w/o selection"), suggesting that even uncoordinated element allocation can slightly improve both energy harvesting and spectral efficiency for systems with few HAPs.

Figure 3 evaluates the impact of increasing the number of HAPs on the spectral efficiency. Our optimized solution maintains superior performance, validating the effectiveness of joint phase-shift and element allocation optimization in multi-HAP scenarios. Among the benchmarks, the random selection scheme once again outperforms the single-HAP dedicated one.

VI. Conclusions

In this work, we studied the benefits of employing a single IRS in a multi-band WPCN for assisting the DL WPT and the UL WIT stages. A practical IRS reflection model was implemented to enable the proposed study. The total data rate maximization problem was formulated with the objective of optimizing the DL WPT time length, the phase-shifts and the distribution of ideal phase-shifts for each WPCN. A solution to the problem was proposed through a decomposition into two subproblems, solved by using successive convex approximation (SCA) for continuous variables and integer linear programming (ILP) solvers for discrete allocation, coordinated via an alternating optimization framework. Simulation results demonstrated significant performance gains of the proposed solution compared to benchmark approaches. The optimized IRS element selection strategy for multi-WPCN operation achieved superior spectral efficiency, outperforming both dedicated single-HAP IRS configurations (where phase-shifts are optimized for only one WPCN) and random element allocation schemes. These improvements validate the importance of coordinated phase-shift optimization and intelligent resource partitioning in multi-band IRS-assisted systems. The results particularly highlight how frequency-selective element assignment enables more efficient spectrum utilization compared to conventional single-band or uncoordinated IRS deployments. As perspectives for this study, we point out the investigation of more sophisticated beamforming design algorithms, and impact of channel estimation errors on performance.

References

[1] A. Ihsan, W. Chen, M. Asif, W. U. Khan, and J. Li, "Energy-Efficient IRS-Aided NOMA Beamforming for 6G Wireless Communications," Mar. 2022, arXiv:2203.16099 [eess]. [Online]. Available: http://arxiv.org/abs/2203.16099

[2] Q. Wu, X. Guan, and R. Zhang, "Intelligent Reflecting Surface-Aided Wireless Energy and Information Transmission: An Overview," *Proceedings of the IEEE*, vol. 110, no. 1, pp. 150–170, Jan. 2022. [Online]. Available: https://ieeexplore.ieee.org/document/9610992/

[3] T. A. Zewde and M. C. Gursoy, "NOMA-based Energy-Efficient Wireless Powered Communications," *IEEE Transactions on Green Communications and Networking*, vol. 2, no. 3, pp. 679–692, Sep. 2018, arXiv:1806.06286 [cs, math]. [Online]. Available: http://arxiv.org/abs/1806.06286

[4] D. Song, W. Shin, and J. Lee, "A Maximum Throughput Design for Wireless Powered Communication Networks With IRS-NOMA," *IEEE Wireless Communications Letters*, vol. 10, no. 4, pp. 849–853, Apr. 2021. [Online]. Available: https://ieeexplore.ieee.org/document/9305257/

[5] Q. Wu, X. Zhou, and R. Schober, "IRS-Assisted Wireless Powered NOMA: Do We Really Need Different Phase Shifts in DL and UL?" *IEEE Wireless Communications Letters*, vol. 10, no. 7, pp. 1493–1497, Jul. 2021. [Online]. Available: https://ieeexplore.ieee.org/document/9400380/

[6] C. A. M. de Pinho and F. R. M. Lima, "Rate maximization with qos guarantees in irs-assisted wpcn-noma systems," in *2022 Workshop on Communication Networks and Power Systems (WCNPS)*. IEEE, 2022, pp. 1–6.

[7] L. Dos Santos Fonseca, F. R. M. Lima, and C. A. M. De Pinho, "Resource Allocation for Spectral Efficiency Maximization in WPCN-NOMA Systems with Multiple IRSs," in *2024 19th International Symposium on Wireless Communication Systems (ISWCS)*. Rio de Janeiro, Brazil: IEEE, Jul. 2024, pp. 1–6. [Online]. Available: https://ieeexplore.ieee.org/document/10639064/

[8] W. Cai, R. Liu, M. Li, Y. Liu, Q. Wu, and Q. Liu, "IRS-Assisted Multicell Multiband Systems: Practical Reflection Model and Joint Beamforming Design," *IEEE Transactions on Communications*, vol. 70, no. 6, pp. 3897–3911, Jun. 2022. [Online]. Available: https://ieeexplore.ieee.org/document/9759366/

[9] A. Salem, K.-K. Wong, C.-B. Chae, and Y. Zhang, "Modeling and Design of RIS-Assisted Multi-cell Multi-band Networks with RSMA," Aug. 2024, arXiv:2408.02160 [eess]. [Online]. Available: http://arxiv.org/abs/2408.02160

[10] F. Yang, R. Deng, S. Xu, and M. Li, "Design and experiment of a near-zero-thickness high-gain transmit-reflect-array antenna using anisotropic metasurface," *IEEE Trans. Antennas Propag.*, vol. 66, no. 6, pp. 2853–2861, Jun. 2018.

[11] P. D. Diamantoulakis, K. N. Pappi, Z. Ding, and G. K. Karagiannidis, "Wireless-Powered Communications with Non-Orthogonal Multiple Access," *IEEE Transaction on Wireless Communications*, vol. 15, no. 12, pp. 8423–8425, Dec. 2016.

[12] H. Ju and R. Zhang, "Throughput Maximization in Wireless Powered Communication Networks," *IEEE Transactions on Wireless Communications*, vol. 13, no. 1, pp. 418–428, Jan. 2014, conference Name: IEEE Transactions on Wireless Communications. [Online]. Available: https://ieeexplore.ieee.org/document/6678102

[13] M. Grant and S. Boyd, "CVX: Matlab software for disciplined convex programming, version 2.1," https://cvxr.com/cvx, Mar. 2014.